(Red color indicating the main revisions)

Flexural fold structures and active faults in the northern-western Weihe Graben, central China

Aiming Lin[1]*, Gang Rao[1,2], and Bing Yan[1,3]

[1]Department of Geophysics, Graduate School of Science, Kyoto University
Kyoto 606-8502, Japan
[2]Department of Earth Sciences, Zhejiang University
Hangzhou 310027, China
[3]Graduate School of Science and Technology, Shizuoka University
Shizuoka 422-8529, Japan

****

***Corresponding author:**
Department of Geophysics
Graduate School of Science, Kyoto University
Kyoto 606-8502, Japan
Tel: 81-75-753-3941
E-mail: slin@kugi.kyoto-u.ac.jp (A. Lin)

Abstract

Field investigations and analyses of tectonic topography related to late Pleistocene–Holocene activity of faults and fault-related flexural folds in the northern–western Weihe Graben, central China, reveal that: (1) four main active faults are present in the study area, the Beishan Piedmont Fault (BPF), the Kouzhen-Guanshan Fault (KGF), the Qishan-Mazhao Fault (QMF), and the Weihe Fault (WF), of which the BPF, KGF, and WF are normal faults whereas the QMF is a left-lateral strike-slip fault; (2) active flexural folds trending ENE–WSW are widely developed on the late Pleistocene–Holocene loess tablelands and alluvial fans, as well as on terrace risers; (3) vertical slip rates on the BPF, KGF, and WF are ~0.5–1.1 mm/yr, and the left-lateral slip rate on the QMF is ~1.5 mm/yr; and (4) a recent seismic faulting event with a magnitude (*M*) >7 occurred in the past ~3000 yr. Our results show that active faults and fault-related flexural folds are developing in the Weihe Graben under an ongoing extensional regime, with listric faulting occurring along pre-existing faults associated with the spreading of continental crust in intracontinental graben systems around the Ordos Block.

Keywords: active normal fault, strike-slip fault, flexural fold, listric fault model, Weihe Graben, Ordos Block

1. Introduction

Intracontinental rift systems generally contain normal faults, fault-related folds that are offset, and deformed sedimentary sequences deposited on basement rocks (e.g., Bradley and Kidd, 1991; Schlische, 1995; McNeill et al., 1997; Yeats et al., 1998; Khalil and McClay, 2002; McCalpin, 2009). However, while active normal faults that developed in extensional environments are widely reported in the literature (e.g., Yeat et al., 1997; Axen, 1999; Cowie and Roberts, 2001; Lin et al., 2013a; Rao et al., 2014), the flexural folds associated with active normal faulting, which record the deformation of unconsolidated sedimentary deposits, are rarely reported.

The Weihe Graben, an intracontinental graben system that has developed in an extensional regime around the Ordos Block, since the Eocene, provides a unique natural laboratory for studying the long-term tectonic history of active normal faults and related flexural fold structures (Fig. 1). Our research has revealed that active normal faults developed in the southeastern Weihe Graben, which are distributed in a zone <500 m wide along the southeastern border of the graben (Rao et al., 2014). These faults are characterized by a distinctive series of stepped fault scarps that dip into the graben at angles of 40°–71°, with an average dip-slip displacement rate of ~2–3 mm/yr (Rao et al., 2014). The slip rates of main active faults in the northern and western graben, the target region of this study, are estimated to be on the order of 0.1–0.5 mm/yr (Xu et al., 1988). However, the deformational features and dynamic mechanisms associated with the active normal faults and fault-related flexural folds developed in the northern and western graben are still unknown, although previous studies have reported the presence of active faults based on geological and geophysical data (e.g., Peng, 1992; Feng et al., 2003; Tian et al., 2003; Deng, 2007; Shi et al., 2009).

Late Pleistocene–Holocene activity on normal faults in the southeastern marginal zone of the Weihe Graben has been described by Rao et al. (2014), and paleoseismicity in this zone has been studied by Rao et al. (2015, this issue). In this study, we focused on active normal faulting and fault-related flexural folds in the northern–western Weihe Graben, adjoining the study area of Rao et al. (2014). We also discuss the formation mechanisms of active fault-related flexural fold structures in the extensional environment of intracontinental grabens around the Ordos Block.

2. Terminology

The term *flexural fold* is a general term used in structural geology to describe flexural flow folds and flexural slip folds in sedimentary rocks with good layering. The deformation mechanisms that produce flexural folds include both folding and slip along layer boundaries, as well as some flow within the layers. In contrast, the term *active flexural fold*, which is used in studies of active tectonics, refers to flexural flow folds developed in weakly consolidated and/or unconsolidated sedimentary deposits during recent geological time. An *active flexural fold*, which is also called an *active flexure,* corresponds to the term *active fault* in Japan (Research Group for Active Faults in Japan, 1991). Generally, it is difficult to recognize whether or not slip has occurred along the boundaries of sedimentary layers in active flexural folds, as deformation in weakly consolidated and/or unconsolidated sediments is often not orderly, and outcrops are often not available for observing flexural slip fold structures in the field. Therefore, in this paper we use the term *flexural fold* to describe all varieties of active flexural folds, including flexural flow and flexural slip folds, folds involving the deformation of weakly consolidated and/or unconsolidated sediments, and folds generating waveform landforms.

3. Tectonic setting

The Weihe Graben is located in the northeast border area of the Tibetan Plateau, at the southern margin of the stable Ordos Block, along a tectonic boundary between the North China Block (NCB) in the north and the Qinling orogenic belt bounded by the South China Block (SCB) in the south (Fig. 1). As a result of crustal extension, the Weihe Graben has received sedimentary deposits since the Eocene of up to ~7000 m in thickness, concomitant with the uplift of mountainous blocks along both the southern and northern borders of the graben (SSB, 1988; Zhang et al., 1998). In the western region, a watershed divide is present along a gap between the Weihe Graben and the Yinchuan Graben, separating the north–northeastward flowing Yellow River and the eastward flowing Weihe River (Fig. 1b). This divide is considered to be the result of folding and uplifting along the northeastern margin of the Tibetan Plateau, as well as rifting around the Ordos Block, which is related to collision between the Indian and Eurasian plates (Lin et al., 2001). Topographically, the graben is sharply bounded by the Qinling Mountains to the south along the northern Qinling Piedmont Fault (QPF), where the topographic relief is on the order of 500 m; in contrast, the northern side of the graben is characterized mainly by deformed and displaced Quaternary loess and alluvial deposits along a gently sloping boundary with the southern margin of the Ordos Block (Fig. 1c; SSB, 1988). Both the Qinling Mountains and the Ordos Block are composed of Precambrian metamorphic basement rocks.

Historical records show that more than 10 large historical earthquakes of $M \geq 7$, including four with $M \geq 8$, have occurred in the graben systems around the Ordos Block; five of those earthquakes occurred in the Weihe Graben (Fig. 1b; SSB, 1988; Deng, 2007). The 1556 M~8.5 Huaxian earthquake, which caused >830,000 deaths, ruptured an active fault zone for up to 70 km along the southeastern margin of the Weihe Graben (e.g., Kuo, 1957; Wang, 1980; SSB, 1988; Xie, 1992; CENC, 2007). Instrumentally recorded earthquakes of $M \geq 5$ have been concentrated in the graben systems around the Ordos Block, but none have been recorded in the interior of the Ordos Block (Fig. 1b). Paleoseismic studies reveal high levels of historical seismicity, and focal mechanisms indicate that normal faults in the Weihe Graben are seismogenically active, under the influence of an intracontinental extensional regime (e.g., SSB, 1988; Zhang et al., 1998; Deng, 2007; Rao et al., 2015, this issue).

4. Flexural folds and active faults

4.1. Topographic features of flexural folds

Active faults and flexural folds were identified in this study by using 30-m-resolution ASTER global digital elevation model (GDEM) data, high-resolution

Google images and field investigations (Figs 1c and 2). Multi-perspective views of the topography made it possible to identify the active faults and tectonic topography of flexural folds more easily than by using traditional methods, such as aerial photographs (Figs 1c and 2).

Topographically, the Weihe Graben is irregular in shape, being narrow in the western area along the course of the Weihe River, and connected with the Shanxi Graben in the east (Fig. 1b and c). In the study area, the graben is linearly bounded by the Qinling Mountains in the south and is irregularly bounded by the Beishan Mountains in the north (Fig. 1c). Loess tablelands, which are extensively developed in the northern portion of the graben, can be divided into two groups: (1) Loess Tableland (I), which formed at 1.3–1.5 Ma, and (2) Loess Tableland (II), which formed at 0.9 Ma (based on stratigraphic sequences and age dating) (Fig. 1c; Feng et al., 2003). These loess tablelands have been deformed into waveform landforms, with a wavelength of ~2–5 km and a wave height of <100 m (generally 20–50 m) (Figs 2–4). Such waveform topography has also been developed on the younger alluvial fans and terraces in the graben (Figs 2 and 3). Stratigraphic sequences reveal that the thicknesses of late Pleistocene loess deposits covering the alluvial and fluviolacustrine sediments on the northern and western side of the Weihe Graben are up to ~150 m (Feng et al., 2003). Both the topographic features and unconsolidated sedimentary sequences indicate that the originally horizontal sediment layers were deformed into waveform folds during the late Pleistocene and Holocene, and that the waveform folds show structural characteristics of active flexural folds, as previously reported from other areas of the world (Yeats et al., 1997). The active flexural folds are mainly distributed in two areas, and enclosed by the main active faults (Figs 1c and 2). Topographically, the ENE-trending waveform belts of the active flexural folds are obliquely truncated at the main active faults, and they appear as echelon patterns in the anticline traces (Fig. 2). The axes of the flexural folds are oriented ENE–WSW, and show continuous individual trends ~5–30 km in length, parallel to the northern margin of the graben (Fig. 2).

The flexural folds of the waveform landforms can also be observed in the field, where they appear as gentle slopes on either sides of the fold axes, with slope angles of 5–10° (Fig. 3). The loess soil layers and old surface soil layers observed in the field appear as anticlinal structures on folds (Fig. 3b).

4.2. Active faults

The analysis of 3D perspectives of GDEM data and Google images, together with field investigations, showed the presence of four main active faults in the study area: the Beishan Piedmont Fault (BPF), the Kouzhen-Guanshan Fault (KGF), the Qishan-Mazhao Fault (QMF), and the Weihe Fault (WF), as well as one inferred fault, the Qinling Piedmont Fault (QPF), located along the southern marginal zone of the Weihe Graben (Fig. 1c). The active faults are all developed along topographic boundaries between the mountains and the graben, and within the loess tablelands, where they are characterized by stepped fault scarps ranging from a few meters up to ~500 m in relief (Figs 1c, 2a, and 4). The BPF and QMF are developed along the boundary between the Beishan Mountains and the Weihe Graben, and the QPF is distributed in the southern marginal zone of the Weihe Graben, bounded by the Qinling Mountains to the south (Fig. 1c). The E–W striking WF mostly follows the course of the Weihe River in the Weihe Graben, from west to east in the study area. The 3D-perspective GDEM data and Google images show that the alluvial fans and terrace risers are not deformed by the QPF, and there is no field evidence (either outcrop or topographic) that indicates recent fault activity, although we have conducted detailed field mapping along the inferred fault trace. Therefore, we infer that the QPF is a blind fault, and we here describe only the structural features of the other four active faults (BPF, KGF, QMF, and WF).

4.2.1. Beishan Piedmont Fault (BPF)

The BPF is located along the northern–northwestern marginal zone of the Weihe Graben, bounded by the Beishan Mountains. The fault strikes SW–NE and extends for >200 km in the study area (Fig. 1c). Topographic profiles show apparent vertical offsets along the BPF of 180–500 m, but offsets are generally in the range of 250–350 m (Fig. 4a–d and 4f–i). Thicknesses of Quaternary sedimentary sequences bounded by the mountains in the northern marginal zone are ~100–200 m (Peng, 1992); therefore, the total vertical offset of the BPF is estimated to be >500 m since the Quaternary. Stepped fault scarps are observed along the fault trend, and are identifiable in the 3D images (Figs 2 and 5).

A fault outcrop is exposed in one of the stepped fault scarps at a construction site

(Fig. 5b and c). The fault cuts the loess soil layers and covering sandy soil layers; it strikes SW–NE and dips to the SE at ~60° (Fig. 5c). The loess soil layers are tilting to the SE at ~5°; the layers contain carbonaceous materials (shells) yielding radiocarbon dating ages of >43,500 yr B.P. (Fig. 5c; Table 1). The sandy soil deposits in the hanging wall of the fault are bedded and contain some gravel layers, indicating an alluvial origin, probably associated with the Jin River (Figs 2b and 5c).

4.2.2. Kouzhen-Guanshan Fault (KGF)

The KGF strikes E–W and extends for ~140 km from the Beishan Mountains to the center of the Weihe Graben (Fig. 1c). The fault cuts through loess tablelands and alluvial fans originating from southeastward flowing rivers, and intersects the escarpment of the Beishan Mountains at an oblique angle (Figs 1c, 2a, and 4a). A continuous fault scarp extends for ~100 km, developed on the Loess Tableland (I) and (II), and on alluvial fans and terrace risers (Figs 4e, f, and 6a). Topographic profiles show that apparent vertical offsets range from 80 m on the alluvial terrace risers to ~340 m on the loess tablelands (Fig. 4e and f). Along the fault scarp, representative outcrops intersecting the fault are found at Locs 3–7, which are described in detail below (Figs 6–8).

Locations 3 and 4 are exposed along the right and left banks of the Yeyu River, along a high fault scarp developed on alluvial terrace risers bounded by the Beishan Mountains (Fig. 6). The fault is exposed at the boundary between basement rocks and alluvial and loess deposits, where the current river forms a waterfall (Fig. 6b–f).

Along both sides of the Yeyu River, the terrace surfaces are ~35–45 m above the current river channel.

A topographic profile shows that the elevations of alluvial terraces on the hanging and footwall sides of the fault are 530 and 430 m (Fig. 4d), respectively, which are comparable with the T2 terrace riser (developed in the area near this site) reported by Xu et al. (1988) in its distribution elevation and height from the current river channel. Based on the stratigraphic sequences and dated ages, the T2 terrace is inferred to have formed during the late Pleistocene (128 ka) (Xu et al., 1988). Thermoluminescence dating of the loess material covering the alluvial deposits of the T2 terrace provides an age of 76 ± 10 ka (Tian et al., 2003). Therefore, we infer that the terrace riser at this location formed during the late Pleistocene, approximately 76–128 ka.

The main fault plane of the KGF strikes E–W and dips south at ~45–60° (Fig. 6b–f); slickenside striations and grooves on the fault plane show a slip vector plunging 85°S, indicating normal slip with a very small horizontal slip component (Fig. 6e–f). The alluvial sediments and loess deposits in the hanging wall are truncated by the fault zone, which is ~50 cm wide and composed of fault breccia and gouge, along which sediment layers are tilted toward the downthrown side; the pebbles in the alluvial sediments are mostly oriented parallel–subparallel to the main fault plane (Fig. 6b–c). These features indicate that the fault is a normal fault dipping toward the Weihe Graben.

Locations 5 and 6 occur on the southern edge of Loess Tableland (II) along the fault scarp on the eastern segment of the KGF, between the Shichuan and Qingyu rivers (Fig. 7; see Fig. 6a for the locations). At Loc. 5, some ground fissures were present under the fault scarp, in a zone <10 m wide (Fig. 7a and b). These ground fissures possess extensional features, including many extensional cracks that had not been filled by surficial materials (Fig. 7b). Creep movement of ground fissures is widespread throughout the Weihe Graben, and is considered to be the result of ground subsidence caused by human activity, not tectonic faulting (Japan–China Cooperative Research Xian Group, 1992). At Loc. 6, the loess deposits are offset by a fault that strikes N30°E and dips SE at 40°. The calcareous materials collected in the loess deposits at both Locs 5 and 6 yield radiocarbon ages of 37,150–37,370 yr B.P. (Fig. 7c, d; Table 1), indicating fault activity in the late Pleistocene–Holocene.

Location 7 occurs at a quarry in alluvial sands and pebbles, exposed on the lowest terrace riser of the Shichuan River along the eastern segment of the KGF (Fig. 8a; see Fig. 6a for the location). Near this location, a fault scarp ~2 m in height (at Loc. 7) on the terrace risers extends continuously for >100 m (Fig. 8a). The fault strikes N64°E and dips southeast at 72°, and cuts alluvial deposits composed of bedded sand pebbles; the pebbles along the fault are mostly oriented parallel–subparallel to the fault plane (Figs 8b, c, and 9). The footwall consists mainly of sand–pebble layers; the hanging wall, in contrast, is composed of interbedded sand and sand–pebble layers containing peaty materials, which yielded a radiocarbon age of 3120 ± 30 yr B.P. (Fig. 9, Table 1). The structural features and ages indicate that a seismic faulting event occurred in the past ~3100 yr, which displaced the alluvial deposits at least ~2 m vertically (Fig. 9).

4.2.3. Weihe Fault (WF)

The WF, developed in the central part of the Weihe Graben, strikes E–W to ENE–WSW; the fault trace roughly coincides with the course of the Weihe River channel, and extends along the Weihe Graben for >250 km (Fig. 1c). The eastern segment of the WF (east of Xian City) is buried, and cannot be recognized from topographic features (Fig. 1c), although geophysical data show a sharp boundary in the isobathic contours of basement rocks, indicating the presence of the fault (Peng, 1992). The western segment (west of Xian City) forms the boundary between loess tableland and lower surfaces formed by Weihe River drainages (Figs 1c and 2b). Topographic profiles show that the loess tablelands have been vertically offset by up to ~55–200 m, with offsets generally being 50–100 m (Fig. 4f–k), and that the upper terrace risers (T2) and lower terrace risers (T0) have been deformed as waveform and offset by ~35 m and ~15 m, respectively (Fig. 10a–d); these data indicate an accumulation of vertical offset on the terrace risers. The fault scarp developed on the lowest terrace riser strikes E–W and is perpendicular to the current channel of the Qihe River (Fig. 10a), and is linked to the high fault scarps developed on the upper terrace (T2); this fault scarp, which can be observed in the field (Fig. 10b–e), is continuous for >5 km. The fault is exposed in three representative outcrops (Locs 9–11), described below.

At Loc. 9, under the fault scarp, the surface soil and underlying sandy soil layers containing gravel have been offset by two faults along which the old brownish surface soil layer and sandy soil layer have been dragged (Fig. 11). Locally, the brownish soil materials are injected as veins into the sandy soil layer, with the veins extending for ~50 cm and terminating sharply; the veins contain organic and peaty materials yielding a radiocarbon age of 3540 ± 30 yr B.P. (Fig. 11b and c; Table 1). Such injection veins in active fault shear zones have been commonly reported elsewhere; they are generally thought to form rapidly during large earthquakes, indicating co-seismic ruptures in a seismogenic fault zone (e.g., Lin et al., 2012, 2013b). The main WF fault plane strikes N38°E and dips SE at 46° (Fig. 11b). The downthrown hanging wall and the deformation features of the dragged old surface soil layer indicate displacement on a normal fault.

Location 10 is on a fault scarp developed on the lowest terrace riser (T1) of the Qihe River (Fig. 10a, c, and e–g). The weakly consolidated alluvial deposits composed of sandy soil with gravel are juxtaposed against unconsolidated surface soils by the fault, which dips at 30–40° (Fig. 10g). The vertical offset of ~14 m, which was measured in a water channel 5 m east of the outcrop (Fig. 10e), is comparable to the height of the fault scarp as measured from the topographic profile (Fig. 10c).

Location 11 is exposed at a construction site on the fault scarp, 10 km west of Loc. 10 (Fig. 10h; see Fig. 2b for location). Weakly consolidated sandy soil is sharply juxtaposed against an unconsolidated surface soil layer by the fault, which strikes N38°E and dips SE at 46° (Fig. 10h).

4.2.4. Qishan-Mazhao Fault (QMF)

Analysis of GDEM data and Google images, together with field investigations, shows that the QMF is mainly located in the northwestern marginal zone of the Weihe Graben (Figs 1c and 12a). The fault strikes WNW–ESE and extends for >120 km, and terminates at the WF in the southeastern portion of the area (Fig. 12a). Topographically, the northwestern segment of the fault follows the boundary between the mountains and Loess Tableland (I), while the eastern segment of the fault cuts Loess Tableland (I) and is characterized by a straight lineament as observed in 3D images (Fig. 12a and c).

Channels of fluvial drainages (R1–R16) cutting across the QMF flow southwestward from the Beishan Mountains and are widespread on Loess Tableland (I); these drainage systems are systematically deflected sinistrally across the fault (Fig. 12b–e). The Wei River (R17), which flows eastward, is also sinistrally offset to the southeast of Loc. 12 (Fig. 12d and e). Channels R1–R8 and R15–R17 are developed on Loess Tableland (I), while channels R9–R14 are developed in the mountains on basement rock. The offsets of sinistrally deflected stream channels were measured along the fault using the perspective view of processed GDEM data (Fig. 12b–e). For river channels without distinct deflection points, the offsets were measured by projecting the trends of both the upstream and downstream sections to the fault trace (Fig.12c and e), using the measurement method of Maruyama and Lin (2000, 2002), with the distance between the respectively projected points representing the amount of offset. Measurement uncertainties result mainly from errors in projecting the drainages to the fault, or to locating the deflections of the points piercing the fault, and are approximately proportional to the amount of deflection. The amounts of sinistral deflection and/or offset of these channels are in the range of 400–3500 m (Fig. 12b–e; Table 2).

Two representative outcrops exposing the QMF are found along a fault scarp near deflected river channels R15–R17, developed on Loess Tableland (I) (Locs 12 and 13; Fig. 12a). Near Locs 12 and 13, the fault scarp facing northeast shows topographic features of waveform landforms similar to those formed by flexural folds, which are observed in the northeastern region of the study area (Fig. 13a and e). At Loc. 12, stepped faults can be observed along the fault scarp (Fig. 13b–d). The alluvial sediment layers, composed of interbedded loess soil and sandy soil layers, are offset by distinct fault planes that dip NE at 40–56° (Fig. 13b–d). At Loc. 13, the fault is exposed at a construction site on a scarp >50 m long (Fig. 13e). The loess deposits and old brownish surface soil layers are dragged and offset by the fault. The sedimentary layers, including the old surface soil layers observed at these two locations, are dragged and offset by the stepped faults, indicating an apparent normal slip component (Fig. 13c-g).

5. Discussion

5.1. Active normal faulting and flexural folding mechanisms

Topographic deformation features associated with active normal faults and fault-related flexural folds are commonly responsible for active fault–fold structures in present-day extensional environments; distinctive features of such structures include the dip angles of normal faults, listric fault geometry, and reverse-drag folds. One characteristic of listric faults developed in graben systems is that, in order to maintain geometric compatibility, sedimentary beds in the hanging wall must rotate and dip towards the fault plane (Fig. 14a and b). Commonly, listric faults involve a number of en echelon faults that sole into a low-angle master detachment (Shelton, 1984).

Geophysical data reveal that active normal faults developed in basin sediments are constrained by pre-existing faults that extend to the lower crust (Peng, 1992). Previous studies have shown that active seismogenic faults with coseismic surface rupture zones mostly develop along pre-existing faults (e.g., Lin et al., 2002, 2009, 2013a, b). The flexural folds developed in basin sedimentary deposits lying on basement rocks are synchronously deformed by listric faulting along preexisting faults accompanying block rotation (Fig. 14a and b). In the study region, the distribution patterns of flexural folds surrounded by active normal faults are, as stated above, indicative of the development of flexural folds constrained mainly by active normal faulting. Seismic reflection profiles across the WF reveal that the near surface Quaternary sedimentary layers of the terrace risers in both sides of the WF have been folded and reversely tilted to the north (Feng et al., 2008; Shi et al., 2008, 2009). Geological data including the drilling data and field investigations show that the fluviolacustrine silt-clay layers overlain by the loess layers have been deformed as an uneven and waveform distribution of the top bedding surface with different elevation in the hanging wall of the WF (Feng et al., 2003). These geophysical and geological data support our findings that the waveform landforms developed on the loess tablelands and alluvial fans, as well as on terrace risers in the Weihe Graben are caused by active flexural-folding.

Topographically, the alluvial fans sourced from the Beishan Mountains are tilted to the south–southeast; however, currently they are tilting towards the north–northwest on the north–northwestern side of fold axes (Figs 1 and 2). Active normal faults, developed on both the northern and southern margins of the Weihe Graben, are characterized by pure dip-slip displacement (Fig. 1c; Rao et al., 2014), indicating a NNW–SSE extensional stress direction, which is consistent with the regional extensional stress direction inferred from earthquake focal mechanisms (Ma, 1989). In contrast, the axes of folds and flexural folds show a general NE–NNE trend, indicating a NW–SE to NNW–SSE compressive stress, which is incompatible with the stress regimes of active faults in the graben. This inconsistency between the stress vectors acting on the normal faults and the flexural folds can be interpreted by a listric fault model based on lithospheric (crustal) thinning of the Weihe Graben relative to neighboring regions (Fig. 14a and b); the thinning is considered to be the result of extension in the lower crust due to underlying asthenospheric mantle flow (Fig. 14c), as revealed by geophysical observations (e.g., Huang et al., 2008; Bao et al., 2011). Our results show that the structural features of the active flexural folds and active normal faults observed in the Weihe Graben are constrained by lithospheric (upper to lower crustal) structures.

5.2. Slip rates of active faults

Previous studies have estimated slip rates on active normal faults in the Weihe Graben, mainly on the faults in the eastern and southeastern portion of the graben (e.g., Li and Ran, 1983; Deng et al., 2003; SSB, 1988); only a few studies, however, have reported the recent activity on the faults in the study area (Xu et al., 1988; Tian et al., 2003). Xu et al. (1988) inferred slip rates on the BPF, KGF, and WF in the study area on the order of 0.1–0.5 mm/yr, based mainly on sedimentary sequence data obtained from drilling records, but without detailed mapping of fault distributions or examination of topographic profile data associated with surface deformation markers. The QMF has been considered as a normal fault, similar to the others developed in the graben (Xu et al., 1988; SSB, 1988; Deng et al., 2003); however, estimates of slip rates on the QMF are still not available because of the paucity of geological data for this fault.

As stated above, the Pleistocene–Holocene terrace risers, alluvial fans, and loess tablelands have all been systematically displaced, and we have used them in this study as topographic surface markers for estimating slip rates. Loess Tableland (I) and (II), which are widely developed in the study area (Figs 2, 6a, and 12a), served as reliable displacement markers in this study, as alluvial sediment layers deposited on the Loess Tablelands (I) and (II) formed in the late Pleistocene, at 1.3–1.5 Ma and 0.9 Ma, respectively (Feng et al., 2003). The alluvial fans and terrace risers developed during the late Pleistocene–Holocene (128–10 ka) in areas along the Weihe River, and its branch streams developed on the loess tablelands are also used as surface displacement markers for estimating slip rates (Figs 6 and 10).

In the northeastern area, in the area of the BPF, the Loess Tableland (II) is vertically offset by 180–500 m (Figs 2a, 4a–c, and 4f–h), indicating a vertical slip rate of 0.18–0.5 mm/yr, which is comparable to the slip rate estimated by Xu et al. (1988). For the KGF, as stated above, the T2 terrace riser that formed in the late Pleistocene (76–128 ka) is offset by ~80 m at Locs 3 and 4 (Figs 4d and 6b–f), corresponding to a vertical slip rate of 0.6–1.1 mm/yr. This value for the slip rate is approximately two times larger than that estimated by Xu et al. (1988). The difference between our results and those of previous studies may be the result of the ages used in the calculations. The slip rates estimated in this study for the BPF and KGF are values averaged over the last ~1 Ma, but Holocene slip rates are not well constrained because of a lack of reliable age dating and fault outcrops. Thus, more work is required to assess the extent of recent activity on these two faults.

The WF was inferred to be a blind active fault with no surface expression (SSB, 1988; Xu et al., 1988), although drilling and seismic profiling reveal the presence of the fault in the subsurface (Shi et al., 2009). Therefore, no data were available in this study for estimating the late Pleistocene–Holocene slip rate of the WF. However, we found that the lowest and highest terrace risers, T0 and T2, are offset by ~15 m and 35 m, respectively, indicating that vertical offset accumulated in these risers, as shown in Fig. 10. The lowest terrace riser is composed of alluvial sandy soil deposits with gravel, but a loess soil layer is absent (see Fig. 10g). The absence of a loess soil layer on the lowest terrace riser indicates that the alluvial deposits formed after the formation of the youngest loess soil layer (called S_0), and thus is inferred from radiocarbon dating to have formed at 10,300 yr B.P. (Liu et al., 1994). Radiocarbon dating of the alluvial sediments at a depth of ~2 m on the terrace riser at Loc. 7 shows an age of ~3120 yr B.P. (Fig 9). Considering the depositional rate of alluvial deposits, we infer that the lowest terrace riser surface formed in the Holocene. Using the upper age limit of 10,300 yr for terrace riser T0 and an offset amount of 15 m measured at Loc. 10, we calculated a vertical slip rate of 1.5 mm/yr for the WF. Our results are comparable with the slip rate of 2-3 mm/yr estimated for the active normal faults in the southeastern Weihe Graben (Rao et al., this issue).

The QMF was inferred to be a normal fault based on the distribution of the features of loess tablelands and strata (SSB, 1988; Feng et al., 2003). However, as stated above, the systematic deflection and/or offset of streams show that the fault is a left-lateral strike-slip fault. Previous study shows that the western Weihe Graben around the QMF is a collision area between the northeastern margin of the Tibetan Plateau and the southwestern corner of the Ordos Block (Lin et al., 2001), and GPS observations along the QMF indicate an eastward to ESE-ward movement of the western side of the QMF (Qu et al., 2014). These data show that the western side of the Weihe Graben is a compressional area under an E-W to ENE-WSW compressive stress that can cause a left-lateral strike-slip component along the NW-trending fault, and therefore support our findings that the QMF is a left-lateral strike-slip fault.

The drainage systems developed along intracontinental fault zones have long been recognized as important and reliable geomorphic markers for understanding the deformational features of active strike-slip faults (e.g., Matsuda, 1967, 1975; Maruyama and Lin, 2000, 2002, 2004; Lin et al., 2002). Deflection patterns of the R1–R8 and R15–R17 stream channels developed on Loess Tableland (I) indicate that the deflections occurred after the formation of Loess Tableland (I), or post 1.3–1.5 Ma (Feng et al., 2003). Using the maximum offsets of 1500–1850 m observed on the R5 and R15 rivers developed on Loess Tableland (I), we calculated a strike-slip displacement rate of ~1–1.5 mm/yr for the QMF.

5.3. Paleoseismicity

Xi'an City, the largest city in the Weihe Graben and one of the ancient capitals of China, has experienced numerous destructive earthquakes during its long history. Historical documents record seven large earthquakes of M>6 in the past ~3000 years, including the1556 M~8.5 Huaxian great earthquake and three large earthquakes (M6.5, 1958; M6.75, 1568; and M7.0, 780 BC) that have occurred in the study area (Xu et al., 1988). Based on the historical records, these three large historical earthquakes are thought to have occurred near the intersection of the KGF and BPF on the eastern segment of the WF, near Xian City, and near the intersection of the QMF and BPF on the western side of the graben (Xu et al., 1988). The study of large-magnitude earthquakes that occurred prior to the availability of routine instrumental measurements is based mainly on historical documents and field observations. Significant uncertainties often exist regarding the locations of epicenters, the magnitudes, and the actual extent of damage (including the number of fatalities), caused by historical earthquakes, as reliable records are generally restricted to settled regions (Lin et al., 2013c). Thus, although the locations of the above three large historical earthquakes (M 6.5, M 6.75, and M 7.0) are uncertain, the inferences about epicentral areas may be reliable on account of the detailed historical documents preserved in the records of the ancient capital of Xi'an City.

As stated above, field evidence shows four main active faults in the study area, cutting the loess tablelands and alluvial deposits, and showing evidence of seismic activity in the late Pleistocene–Holocene. At Loc. 7, the KGF cuts alluvial deposits of the lowest terrace with a vertical offset of ≥2 m, and the calcium material in the deposits yielded a radiocarbon age of 3120 yr B.P. (Fig. 9; Tables 1 and 2); this indicates that the lowest terrace riser formed in the late Holocene. The presence of a 2-m-high fault scarp cutting the lowest terrace riser at Locs 5–7 shows that a faulting event occurred since the formation of the terrace riser (Figs 6a and 7–10). A previous study showed that surface rupturing in the graben systems around the Ordos Block is generally related to *M*>7 earthquakes (SSB, 1988). Accordingly, we infer that a large seismic faulting event with a magnitude of M >7 occurred on the KGF sometime since 3120 yr B.P..

Recent activity on the WF can be inferred from data at Locs 9–11, where old surface soil materials included in loess deposits and the lowest terrace risers are offset by the fault (Figs 9–11). At Loc. 9, two surface soil layers are interbedded with the loess layers, which are all offset by two faults (Fig. 11). Radiocarbon dating shows that one of the old surface soil layers formed at ~3520 yr B.P. (sample no. 20140910; Table 1), indicating that at least one faulting event has occurred on the WF since 3520 yr B.P. (Fig. 11; Table 1). The timing of this event is similar to that inferred for the KGF (Loc. 7), but we have no evidence that the faulting in the two locations was caused by the same event. Also, we do not know whether either of these two events correspond to the 1568 M 6.5 earthquake that occurred in the northern marginal zone of the graben (Fig. 1b). Therefore, more work is required to fully understand the details associated with paleo- and historical earthquakes, and to understand which active fault might have triggered the 1568 event; such studies are warranted by the seismic hazards that are present in this densely populated region.

6. Conclusions

We have reached the following conclusions based on an analysis of remote-sensing images, field investigations, and derived radiocarbon ages.

1) Four main active faults are present in the study area: the Beishan Piedmont Fault (BPF), the Kouzhen-Guanshan Fault (KGF), the Qishan-Mazhao Fault (QMF), and the Weihe Fault (WF). The BPF, KGF, and WF are normal faults, while the QMF is a left-lateral strike-slip fault.
2) Active flexural folds trending ENE–WSW are widely developed on the late Pleistocene–Holocene loess tablelands and alluvial fans and terrace risers; these folds probably formed by active listric faulting associated with the spreading of continental crust in the intracontinental graben systems around the Ordos Block.

3) Vertical slip rates on the active normal faults (BPF, KGF, and WF) are estimated to be ~0.5–1.1 mm/yr, and the horizontal slip rate on the active left-lateral strike-slip fault (QMF) is estimated to be ~1.5 mm/yr.
4) The most recent seismic faulting event in the study region, with a magnitude of $M > 7$, is inferred to have occurred during the last ~3000 yr.

Our results reveal that the structural features of active flexural folds and normal faults observed in the study area are constrained by lithospheric structures in the upper to lower crust and tectonic movements in neighboring regions.

Acknowledgements

We are grateful to two anonymous reviewers for their critical reviews that helped to improve a previous version of this manuscript. We thank Z. Ren, J. Hu, J. Fu, J. Du, H. Chen, and W. Gong for their assistance in the field. We also thank Earth Remote Sensing Data Analysis Center (ERSDAC) for making ASTER GDEM data freely available from their web site. This work was supported by a Science Project grant (Project no. 23253002, awarded to A. Lin) from the Ministry of Education, Culture, Sports, Science and Technology of Japan.

References

Axen, G.J., 1999. Low-angle normal fault earthquakes and triggering. Geophysical Research Lettes 26, 3693–3696.

Bao, X., Xu, M., Wang, L., Mi, N., Yu, D., Li, H., 2011. Lithospheric structure of the Ordos Block and its boundary areas inferred from Rayleigh wave dispersion. Tectonophysics 499, 132–141.

Bradley, D.C., Kidd, W.S.F., 1991. Flexural extension of the upper continental crust in collisional foredeeps. Geoogical Society of America Bulletin 103, 1416–1438.

CENC (China Earthquake Networks Center), 2007. The 1556 Huaxian great earthquake, Shaanxi, China: the largest total of fatalities ever claimed (in Chinese). Available online at: http://www.csi.ac.cn/manage/html/4028861611c5c2ba0111c5c558b00001/_history/hxz/qyzhenhai/zh20060609002.htm (Last accessed 10 Nov. 2014)

Cowie, P.A., Roberts, G.P., 2001. Constraining slip rates and spacings for active normal faults. Journal of Structural Geology 23, 1901–1915.

Deng, Q., 2007. Active Tectonics Map of China, Seismological Press (in Chinese).

Deng, Q., Zhang, P., Ran, Y., Yang, X., Min, W., Chu, Q., 2003. Basic characteristics of active tectonics of China. Science In China Series D 46, 356–372.

Feng, X., Tian, Q., Sheng, X., 2003. Analysis of activity difference of the west section of the Weihe fault. Geol. Rev. 49, 233–238. (in Chinese with English abstract)

Feng, X., Li, X., Ren, J., Shi, Y., Dai, W., Wang, F., Mian, K., Han, H., 2008. Manifestations of Weihe fault at deep, middle, shallow and near-surface depth.

Seismology and Geology 30, 364-272.

Huang, Z., Xu, M., Wang, L., Mi, N., Yu, D., Li, H., 2008. Shear wave splitting in the southern margin of the Ordos Block, north China. Geophysical Research Letters 35, L19301. http://dx.doi.org/10.1029/2008GL035188

Japan-China Cooperative Research Xian Group, 1992. Active Faults in the Weihe Basin and Ground Fissures in Xian City, Shaanxi Province, China: A Report on the Japan-China Cooperative Studies on Earthquake Prediction (1987-1989). Bulletin of Earthquake Research Institute, University of Tokyo, 7, 1–186. http://hdl.handle.net/2261/13832 (in Japanese with English abstract)

Khalil, S.M., McClay, K.R., 2002. Extensional fault-related folding, northwestern Red Sea, Egypt. Journal of Structural Geology 24, 743–762.

Kuo, T., 1957. On the Shensi earthquake of January 23, 1556. Acta Geophysica Sinica, 6, 59–68. (in Chinese with English abstract)

Li, X., Ran, Y., 1983. Active faults along the north margins of Huashan and Weinan Loess Tableland. North China Earthquake Science 1, 10–18. (in Chinese with English abstract)

Lin, A., Yang, Z., Sun, S., and Yang, T., 2001. How and when did the Yellow River develop its square bend? Geology 29, 951–954.

Lin, A., Fu, B., Guo, J., Zeng, Q., Dang, G., He, W., Zhao, Y., 2002. Co-seismic strike-slip and rupture length produced by the 2001 M_s 8.1 central Kunlun earthquake. Science 296, 2015–2017.

Lin, A., Ren, Z., Jia, D., Wu, X., 2009. Co-seismic thrusting rupture and slip distribution produced by the 2008 M_w 7.9 Wenchuan earthquake, China. Tectonophysics 471, 203–215.

Lin, A., Shin, J., Kano, K., 2012. Fluidized cataclastic veins along the Itoigawa-Shizuoka Tectonic Line Active Fault System, Central Japan, and Its seismotectonic implications. Journal of Geology 120, 453–465.

Lin, A., Toda, S., Rao, G., Tsuchihashi, S., Yan, B., 2013a. Structural analysis of Coseismic normal fault zones of the 2011 M_w 6.6 Fukushima earthquake, Northeast Japan. Bulletin of Seismological Society of America 103, 1603–1613.

Lin, A., Yamashita, K., Tanaka, M., 2013b. Repeated seismic slips recorded in ultracataclastic veins along active faults of the Arima–Takatsuki Tectonic Line, southwest Japan. Journal of Structural Geology 48, 3–13.

Lin, A., Rao, G., Hu, J., Gong, W., 2013c. Reevaluation of the offset of the Great Wall caused by the ca. M 8.0 Pingluo earthquake of 1739, Yinchuan graben, China. Journal of Seismology 17, 1281–1294.

Liu, J., Chen, T., Song, C., Guo, Z., Li, K., Gao, S., Qiao, Y., Ma, Z., 1994. Datings and reconstruction of the high resolution time series in the Wehnan loess section of the last 150000 years. Quaternary Science 3, 193–202.

Ma, X., 1989. Lithospheric Dynamics Atlas of China (in Chinese). China Cartographic Publishing House, Beijing, 548 pp.

Maruyama, T., Lin, A., 2000. Tectonic history of the Rokko active fault zone (southwest Japan) as inferred from cumulative offsets of stream channels and basement rocks. Tectonophysics 323, 197–216.

Maruyama, T., Lin, A., 2002. Active strike-slip faulting history inferred from offsets of topographic features and basement rocks: a case study of the Arima-Takatsuki Tectonic Line, southwest Japan. Tectonophysics 344, 81–101.

Maruyama, T., Lin, A., 2004. Slip sense inversion on active strike-slip faults in southwest Japan and its implications for Cenozoic tectonic evolution. Tectonophysics 383, 45–70.

Matsuda, T., 1967. Strike-slip faulting along the Atotsugawa fault, Japan. Bulletin of the Earthquake Research Institute, University of Tokyo 44, 1179–1212. (in Japanese with English abstract)

Matsuda, T., 1975. Active fault assessment for Irozaki fault system, Izu Peninsula, in: Tsuchi, R. (Ed.), Reports on the Earthquake off the Izu Peninsula, 1974, and the Disaster, pp. 121–125. (in Japanese with English abstract)

McCalpin, J.P., 2009. Paleoseismology, second edition. International Geophysics Series, vol. 95, Academic Press 613 pp.

McNeill L.C., Kenneth, A.P., Goldfinger, C., Kulm, L.D., Yeats, R., 1997. Listric normal faulting on the Cascadia continental margin. Journal of Geophysical Research 102, B6, 12123–12138.

Peng, J., 1992. Tectonic evolution and seismicity of Weihe fault zone. Seismology and Geology 14, 113–120. (in Chinese with English abstract)

Qu, W., Lu, Z., Zhang, Q., Li, Z., Penf, J., Wang, Q., Drummond, J., Zhang, M., 2014. Linematic model of crustal deformation of Fenwei basin China based on GPS observation. Journal of Geodynamics,, 75, 1-8.

Rao, G., Lin, A., Yan, B., Jia, D., Wu, X., 2014. Tectonic activity and structural features of intracontinental active normal faults in the Weihe Graben, central China. Tectonophysics 636, 270–285.

Rao, G., Lin, A., Yan, B., 2015. Paleoseismic study on the active normal-faults in the southeastern Weihe Graben, central China. Journal of Asian Earth Sciences, this issue.

Research Group for Active Faults of Japan (RGAFJ) (1991). Active faults in Japan—Sheet maps and inventories (revised edition), Univ. Tokyo Press, Tokyo, 437pp. (in Japanese with English summary)

Schlische, R. W., 1995. Geometry and origin of fault related folds in extensional settings. AAPG Bulletin 79, 1661–1678.

Shelton, J.W., 1984. Listric normal faults; an illustrated summary. AAPG Bulletin 68, 801–815.

Shi, Y., Feng, X., Dai, W., Run, J., Li, X., Han, H., 2008. Distribution and structural characteristics of the Xi'an section of the Weihe fault. Acta Seismologica Sinica 30, 634-647. (in Chinese with English abstract)

Shi, Y., Feng, X., Chong, J., Bian, J., Zhang, A., Xu, G., Dai, W., Li, X., 2009. Seismology and Geology 31, 9–21. (in Chinese with English abstract)

State Seismological Bureau (SSB), 1988. Active fault system around Ordos Massif (in Chinese). Seismological Press, Beijing, 352 pp.

Stuiver, M., Reimer, P.J., Reimer, R., 2003. CALIB radiocarbon calibration version 4.4. http://radiocarbon.pa.qub.ac.uk/calib/ (Last accessed, 20 March 2014).

Tian, Q., Shen, X., Feng, X., Wei, K., 2003. Primary study on Quaternary tectonic events based on variation of fault activity in Weihe basin. Seismology and Geology 25, 146–154. (in Chinese with English abstract)

Wang, J., 1980. Ground ruptures during the large earthquake of 1556, Huaxian County, Shanxi. Acta Seismologica Sinica 2, 430–437. (in Chinese with English abstract)

Wang, J., 1987. The Fenwei rift and its recent periodic activity. Tectonophysics 133, 257–275.

Xie, Y., 1992. On magnitude of 1556 Guanzhong great earthquake. Journal of Catastrophology 7, 10–13. (in Chinese with English abstract).

Xu, Y., Shen-tu, B., Wang, Y., 1988. A preliminary study of the characteristics of the activity of the northern boundary fault belt of Weihe basin. Seismology and Geology 10, 77–88. (in Chinese with English abstract)

Yeats, R., Seih, K., Allen, C., 1997. The Geology of earthquakes. Oxford University Press, Oxford, 568 pp.

Yeats, R., Kulm, L. D., Goldfringer, C., McNeil, L.C., 1998. Stonewall anticline: An active fold on the Oregon continental shelf. Geological Society of America Bulletin 110, 572–587.

Zhang, Y., Mercier, J.L., Vergély, P., 1998. Extension in the graben systems around the Ordos (China), and its contribution to the extrusion tectonics of south China with respect to Gobi-Mongolia. Tectonophysics 285, 41–75.

Figure captions

Figure 1. (a) Location map of the Weihe Graben, showing the distribution of major active faults and large historical earthquakes in the graben systems around the Ordos Block; modified from Deng (2007). (b) Inset map showing the tectonic background. ATF, Altyn Tagh Fault; HYF, Haiyuan Fault; KLF, Kunlun Fault; GZ-YSF, Ganzi-Yushu Fault; XSHF, Xianshuihe Fault; SCB, South China Block; NCB, North China Block; LSTB, Longmen Shan Thrust Belt. (c) Color-shaded relief map showing the location and topographic features of the study area. The red star indicates the epicenter of the 1556 *M*~8.5 Huaxian earthquake (SSB, 1988; CENC, 2007). HPF, Huashan Piedmont Fault; NMF–WLT, North Margin Fault of the Weinan Loess Tableland; BPF, Beishan Piedmont Fault; QPF, Qinling Piedmont Fault; KGF, Kouzhen–Guanshan Fault; WF, Weihe Fault; QMF, Qishan-Mazhou Fault. LT(I), Loess Tableland (I); LT(II), Loess Tableland (II).

Figure 2. Color-shaded relief maps derived from 30-m resolution ASTER GDEM data showing the distribution of active faults and topographic features in the northeastern (a) and central (b) areas of the study region. (a) Northeastward perspective view of the area to the west of Yanliang City. (b) Northward perspective view of the area west–southwest of Kouzhen. The waveform flexural folds are formed on Loess Tableland (I) and (II) and on alluvial fans (terrace risers).

Figure 3. Field photographs showing topographic features representative of flexural

folds, observed at Locs 1 (a), 2 (b), and 9 (c, d). The waveform landforms observed at Locs 1 and 2 are developed on Loess Tableland (I), and at Loc. 9 on Loess Tableland (II) (see Figs 1 and 2 for locations).

Figure 4. Topographic profiles across the active faults (see Fig. 1 for locations). Lt-I, Loess Tableland (I); Lt-II, Loess Tableland (II); BPF, Beishan Piedmont Fault; QPF, Qinling Piedmont Fault; KGF, Kouzhen–Guanshan Fault; WF, Weihe Fault; QMF, Qishan-Mazhou Fault.

Figure 5. Field photographs showing topographic features representative of stepped faults (a) and fault outcrops (b) (Loc. 8; see Fig. 2 for location). Person for scale (b).

Figure 6. (a) Color-shaded relief maps derived from 30-m resolution ASTER GDEM data, showing the topographic features of the Kouzhen-Guanshan Fault (KGF). (b–f) Field photographs of the KGF fault outcrops. (b, c) Location 3; scale given by people at the top of the outcrop (b) and by the 35-cm long hammer (c). (d–f) Location 4. The foliated fault breccia and cataclasite zone is bounded by distinct fault planes that dip SW at angles of 40–50°. People for scale. (g) Lower hemisphere equal-area stereographic projection showing the orientations of striations on the fault surface in (f). Long arrow indicates the movement sense of the hanging wall.

Figure 7. Field photographs of the Kouzhen-Guanshan fault outcrops. (a, b) Location 5. Note the ground fissures in the footwall of the fault scarp. (c, d) Location 6. Scale given by people (a, c) and a 2-m long measuring rod (b, d).

Figure 8. Field photographs of the Kouzhen-Guanshan Fault (KGF) fault outcrop at Loc. 7. (a) Overview of the fault outcrop. (b) Fault exposed in the 2-m-high fault scarp. (c) Close-up view of (b).

Figure 9. Location 7. (a) Exposure of the KGF. (b) Corresponding sketch of (a). Unit 1, sand with pebbles; Unit 2, sand–pebble deposit; Unit 3, fine-grained sand; Unit 4, fine-grained sand with organic and peat soil. Ruler for scale is 2 m in length.

Figure 10. (a) Color-shaded relief maps derived from 30-m resolution ASTER GDEM data, showing the distribution of the WF and the deformation features of terrace risers (see Fig. 2b for the location). (b–d) Topographic profiles across fault traces. Field photographs of fault outcrops at Loc. 10 (e–g) and Loc. 11 (g). The terrace riser (T2) has been deformed as waveforms.

Figure 11. Field photographs of outcrop of the WF at Loc. 9. (a) The fault is exposed under the fault scarp. (b) Close-up view of (a); note that the old surface soil is dragged along the fault surface. (c) Injection soil veins in the fault zone shown in (b). The person shows the scale. The radiocarbon age of the sand soil vein is 3520 ± 30 yr B.P. (Table 1), indicating activity on the fault since the late Holocene.

Figure 12. (a, b, d) Color-shaded relief maps derived from 30-m resolution ASTER GDEM data, showing the topographic features of the Qishan-Mazhao Fault (QMF). (c, e) Interpretation maps of (b) and (d), respectively. R1–R17 are the deflected stream channel drainages and Hr3–Hr15 are the offset amounts of

R3–R15, respectively (see Table 2 for details).

Figure 13. Field photographs of fault outcrops at Loc. 12 (a–d) and Loc. 13 (e–g) along the Qishan-Mazhao Fault (QMF). (a) Southward view of the fault scarp (taken near Loc. 12). Note that the fault scarp is facing northeastward. (b) Stepped faults exposed along the fault scarp of the QMF (near Loc. 12). (c, d) Stepped faults exposed at Loc. 12. (e) Fault scarp facing northeast (Loc. 13). (f, g) Close-up views of the fault outcrop at Loc. 13.

Figure 14. Listric fault model (a, b) and mode of tectonic deformation for the Weihe Graben (c). (a) Pre-existing listric faults in basement rock. (b) Activation of pre-existing listric faults rotates the blocks. (c) Landscape of the Weihe Graben is controlled by intracontinental normal faulting, resulting in large amounts of subsidence and the accumulation of a thick section of sediments in the rift basin. Subsurface structures are modified from Wang (1987) and SSB (1988). Active normal faults and flexural folds in the study area are formed in a regime of ongoing extension that is probably related to the pre-existing spreading and rifting of the continental crust in this area (in contrast to the Ordos Block and other neighboring orogenic regions). The lithospheric structures are schematic and based on the geophysical data of Bao et al. (2011). The vertical scale is not precise.

Figure1

Click here to download high resolution image

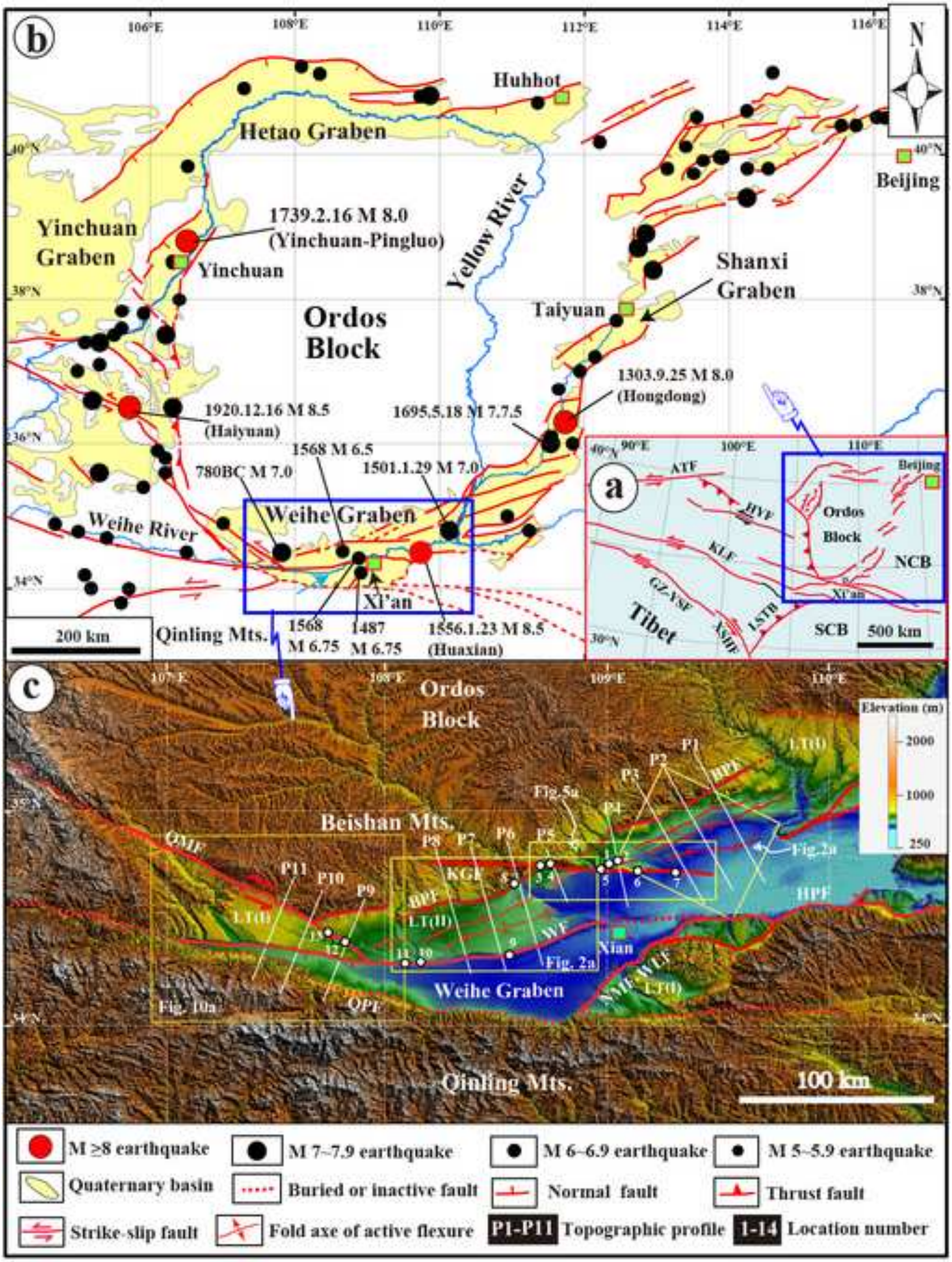

Figure2

Click here to download high resolution image

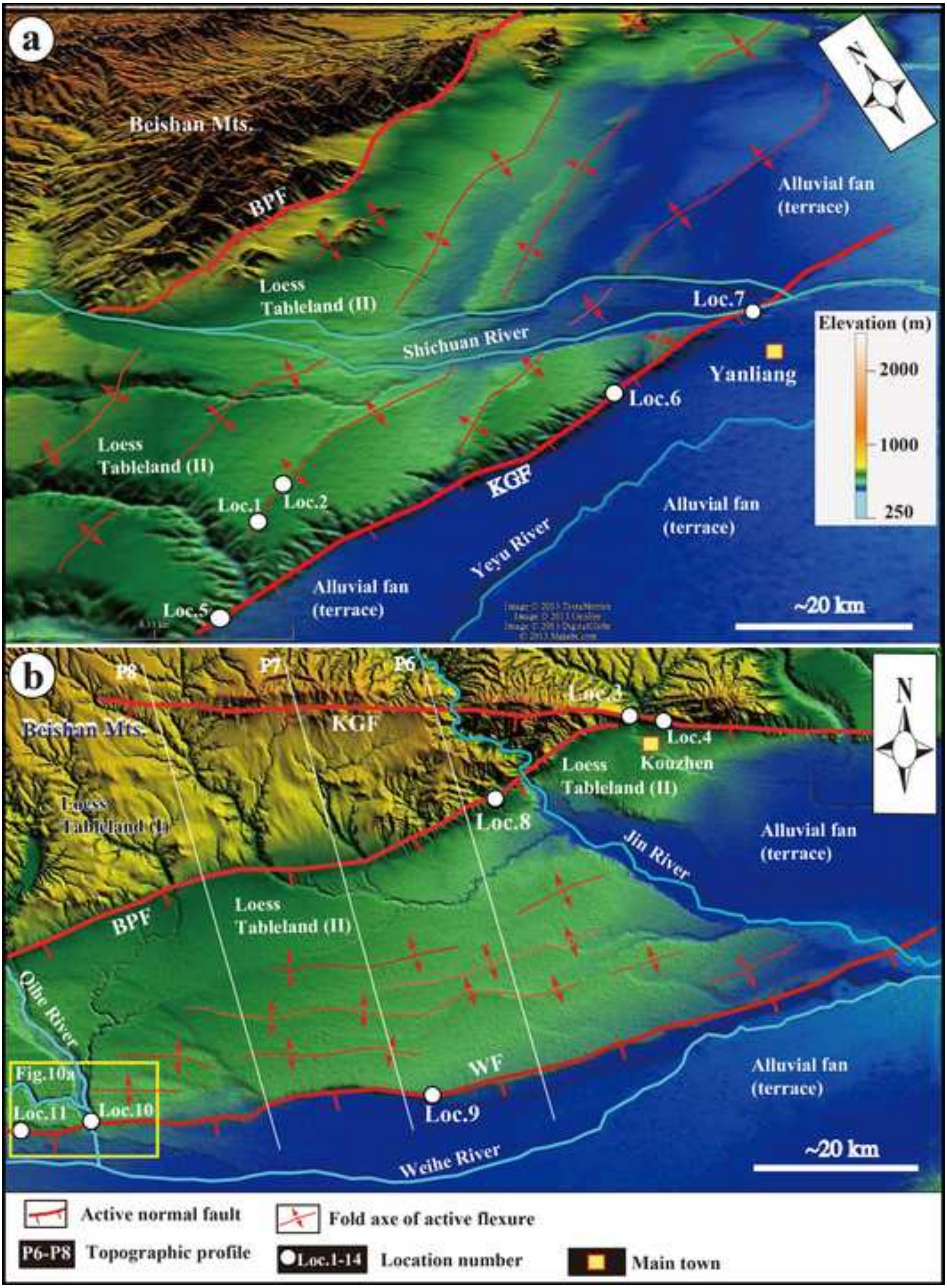

Figure3

Click here to download high resolution image

Figure4

Click here to download high resolution image

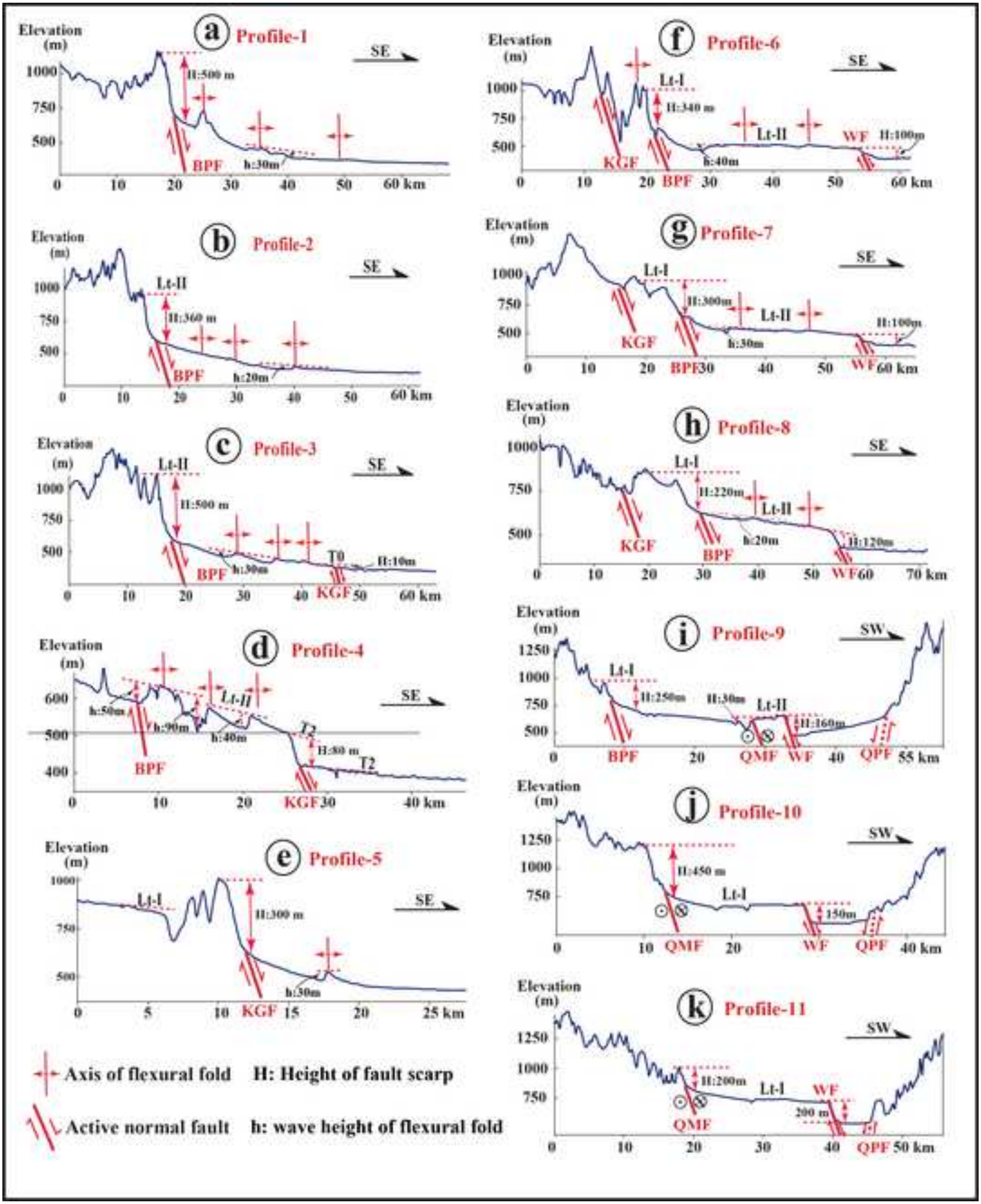

Figure5

Click here to download high resolution image

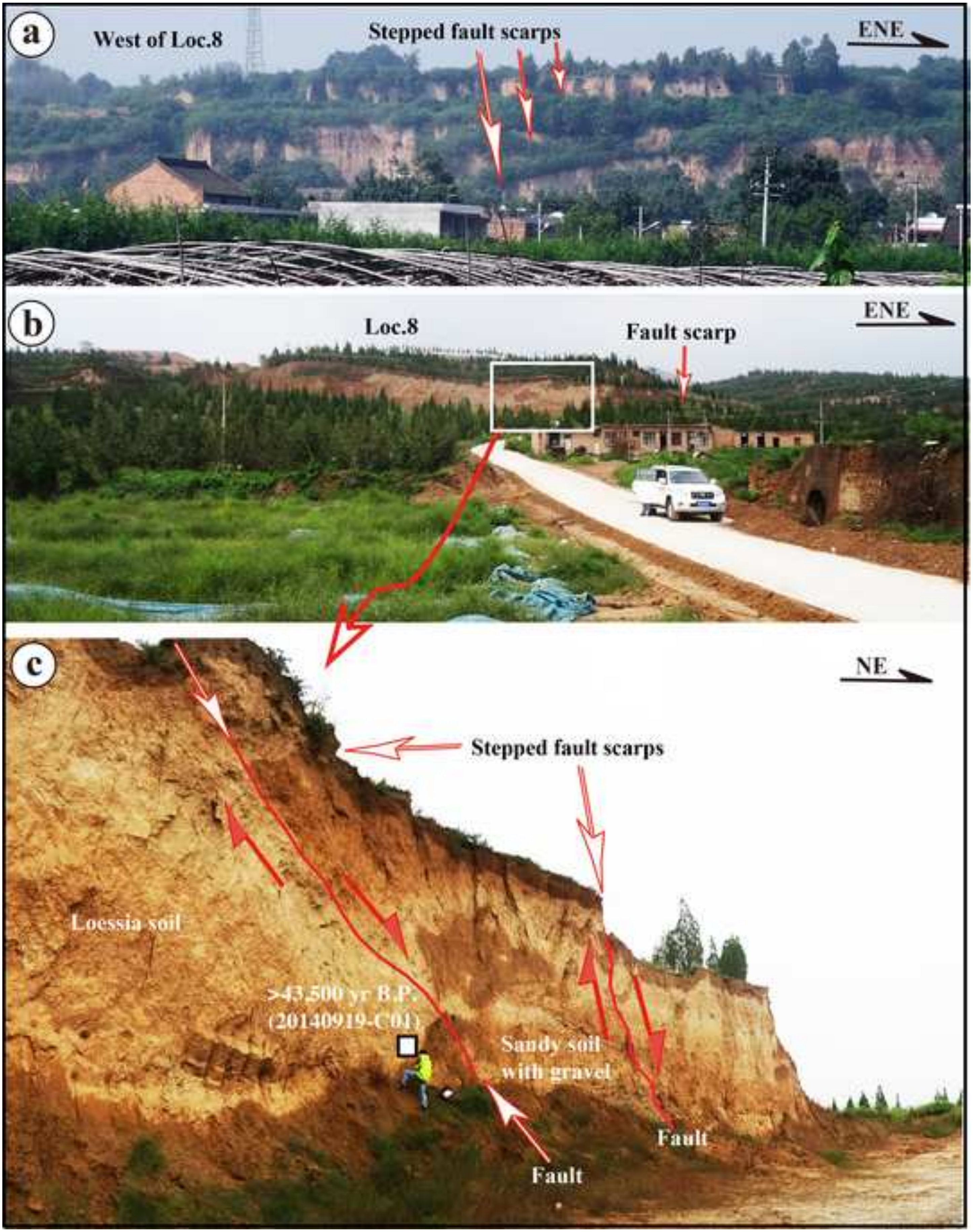

Figure6
Click here to download high resolution image

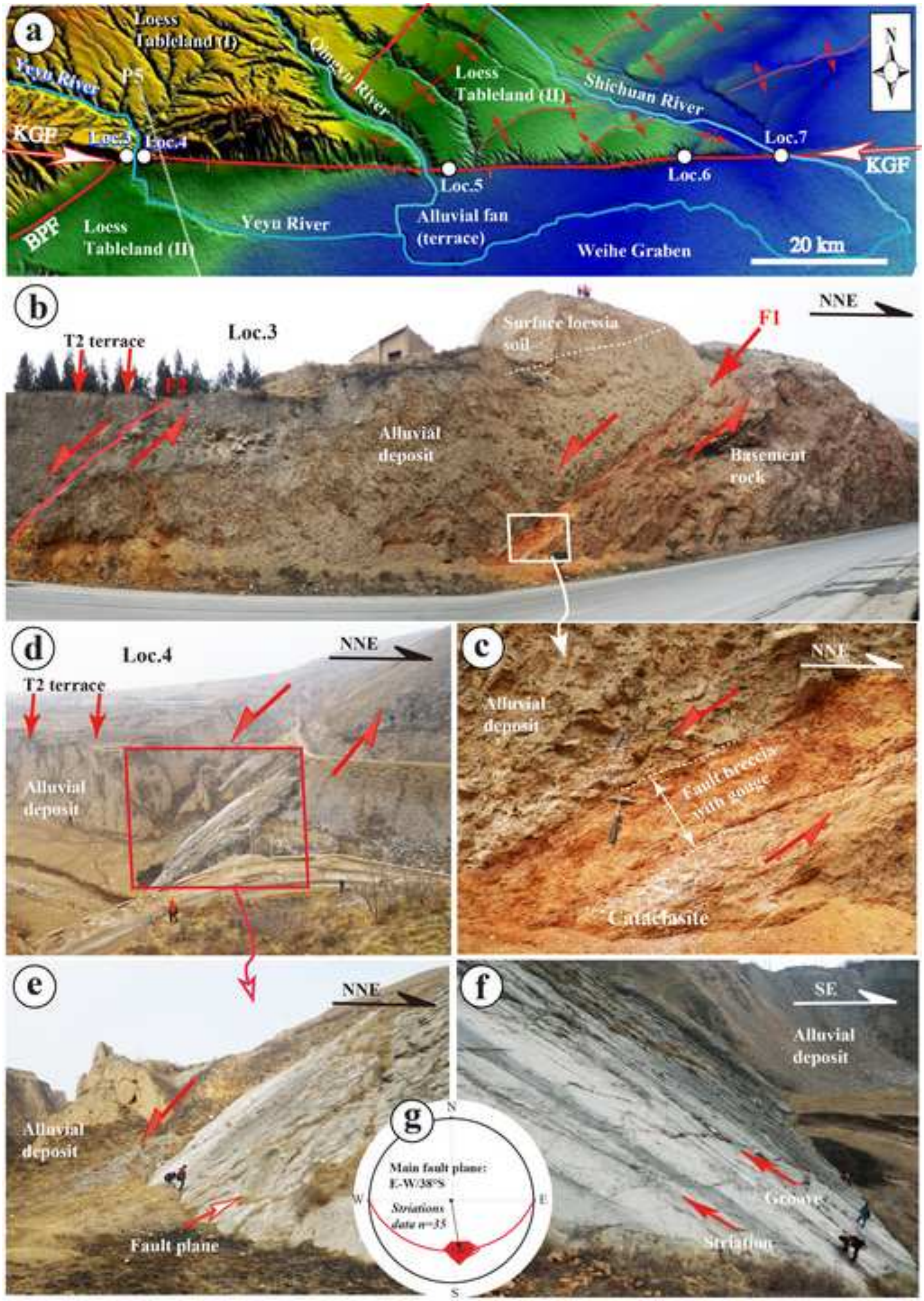

Figure7

Click here to download high resolution image

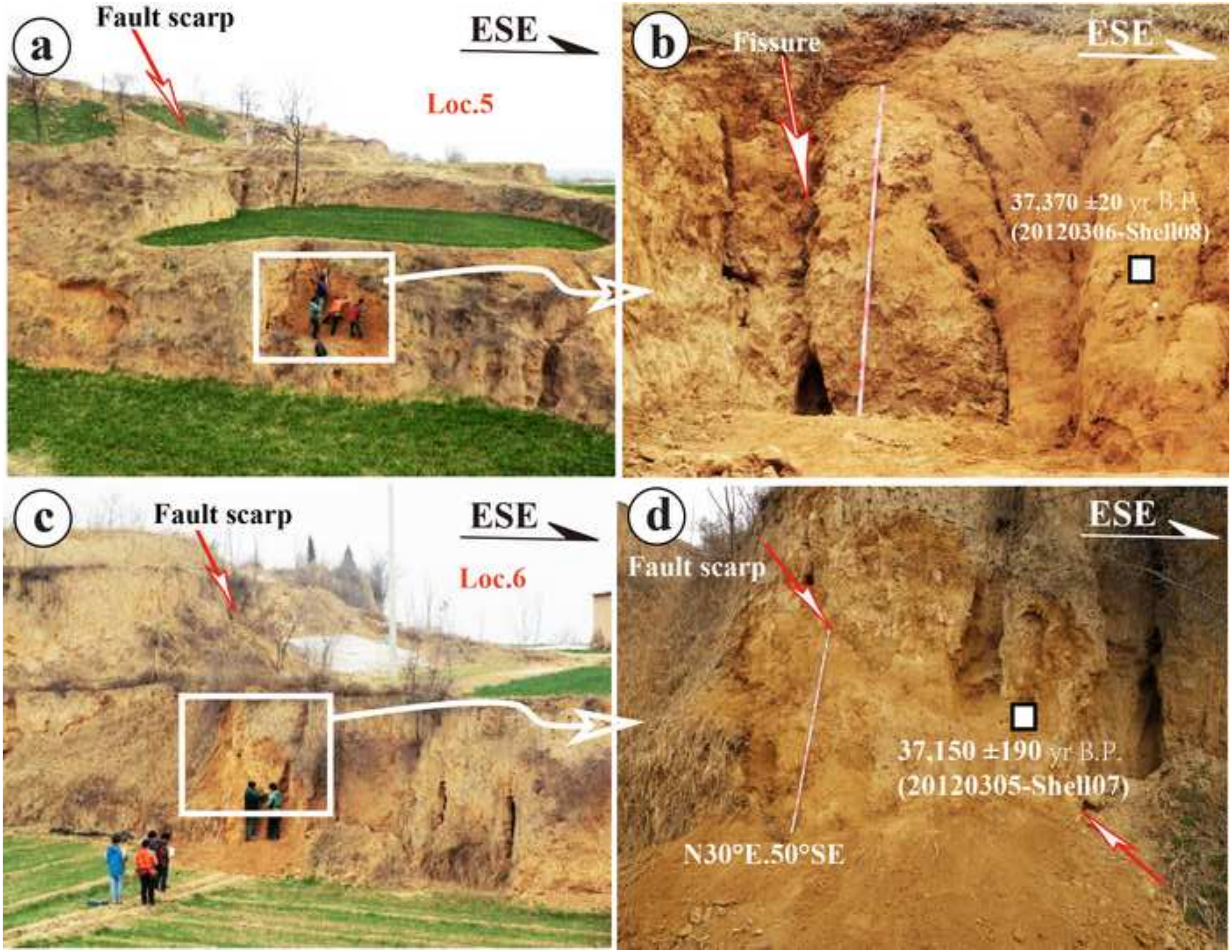

Figure8

Click here to download high resolution image

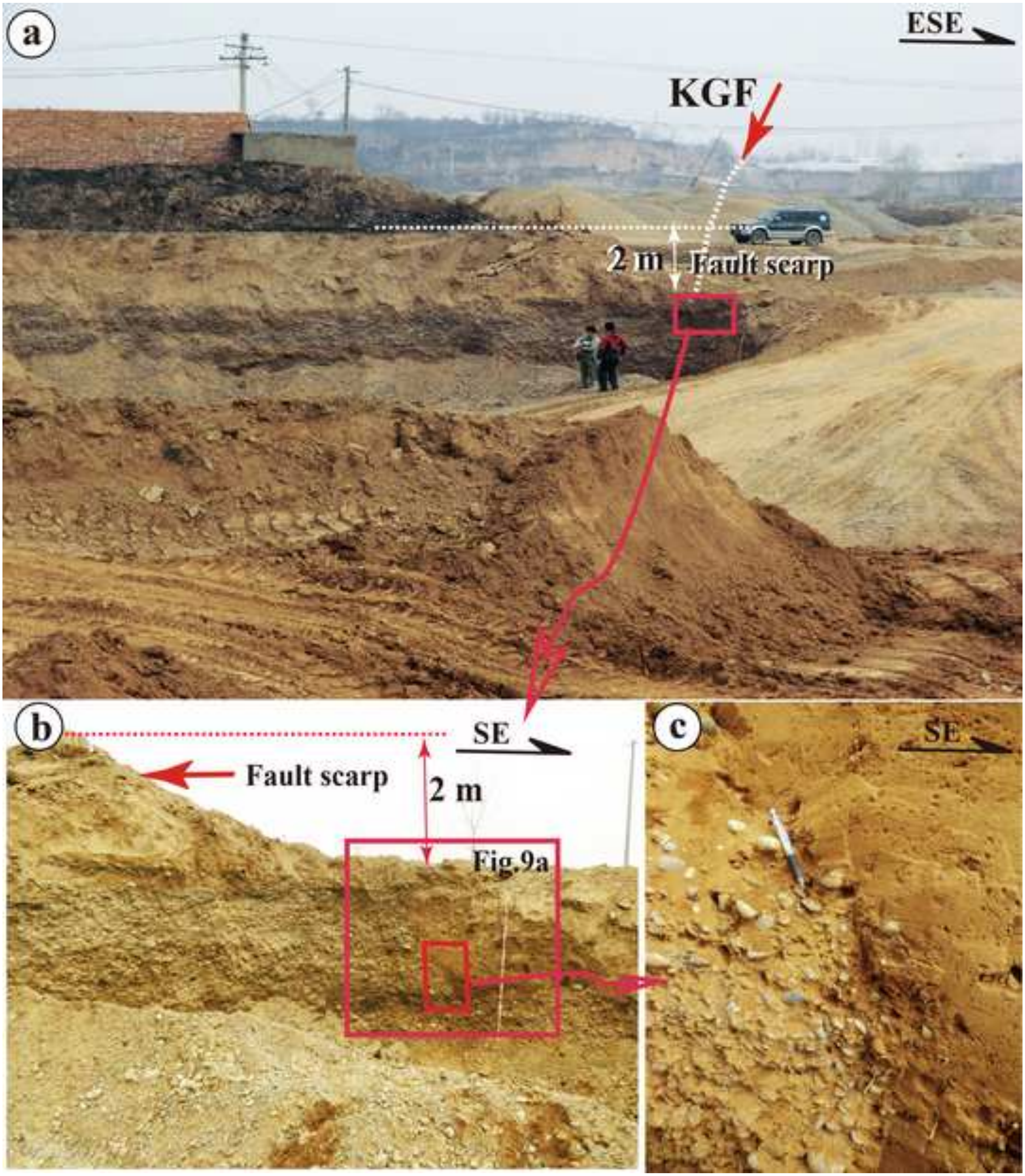

Figure9
Click here to download high resolution image

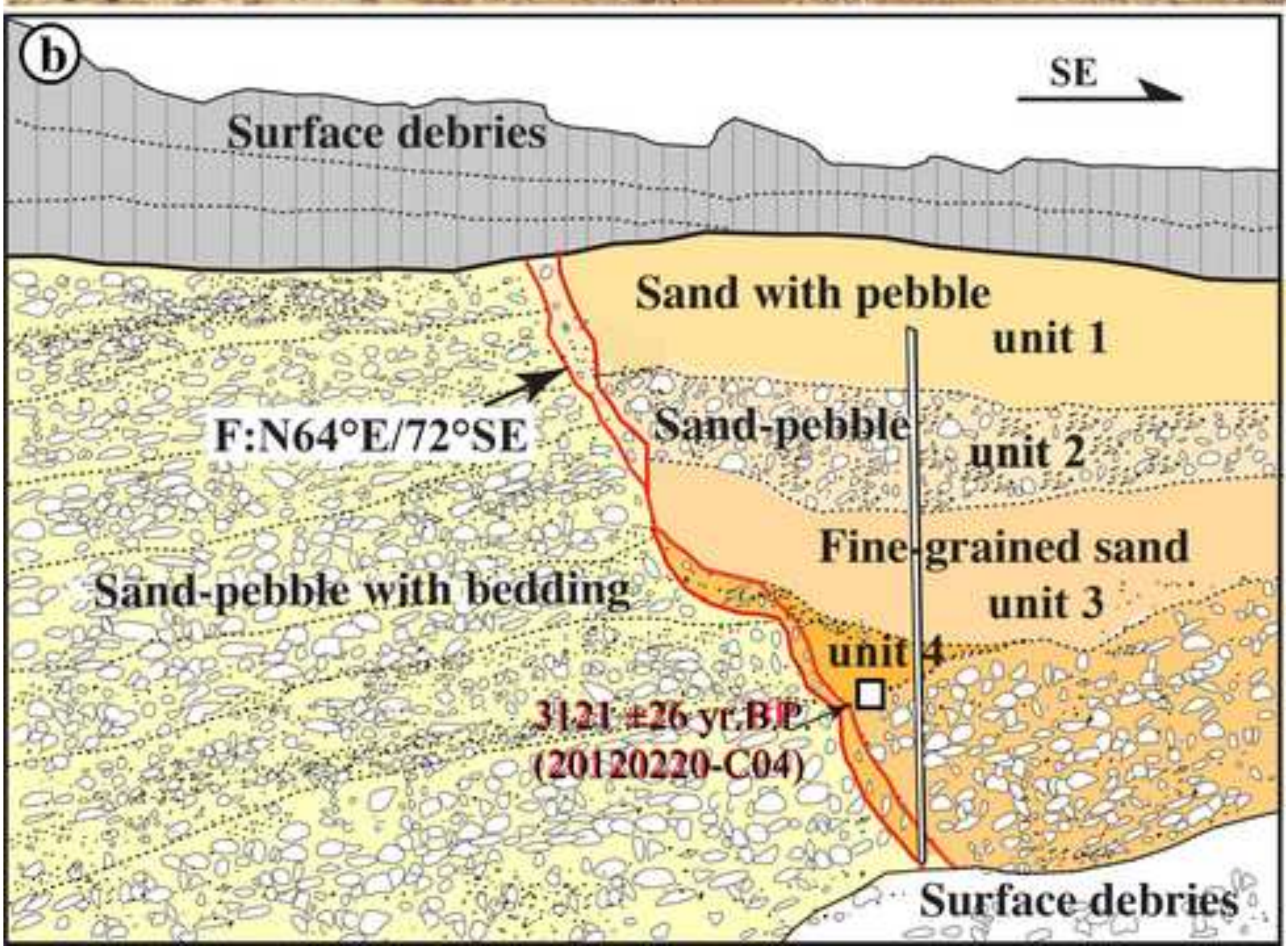

Figure10
Click here to download high resolution image

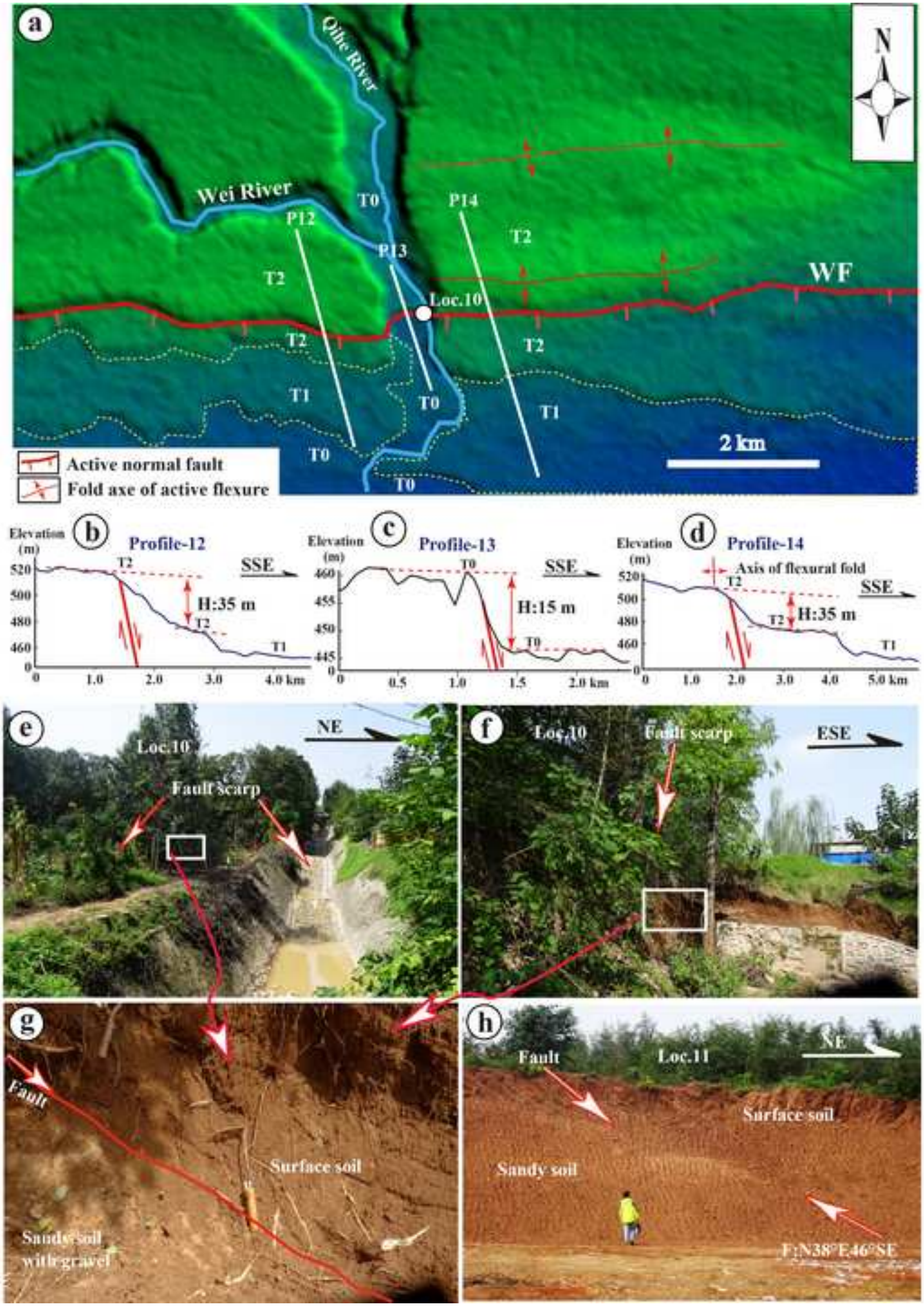

Figure 11

Click here to download high resolution image

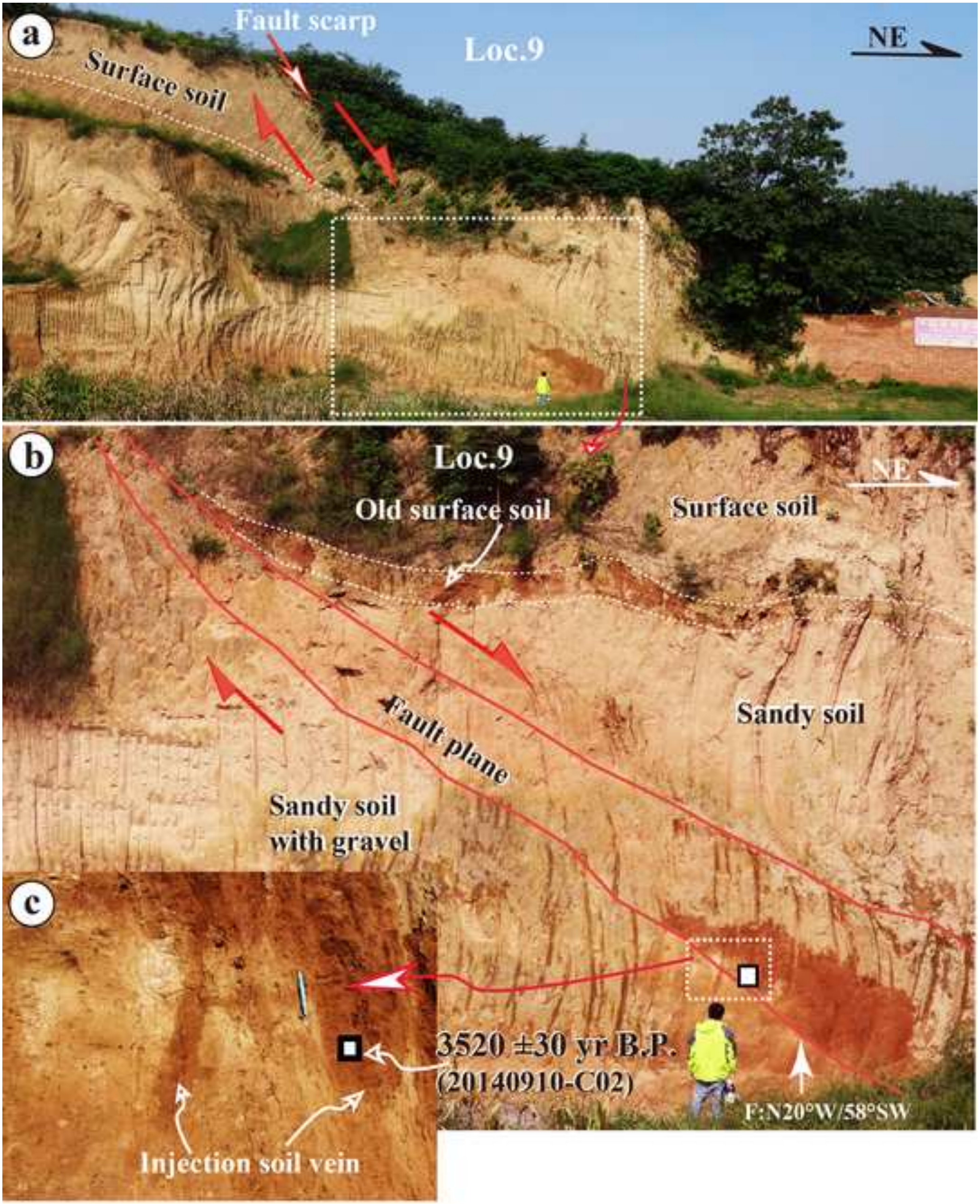

Figure12

Click here to download high resolution image

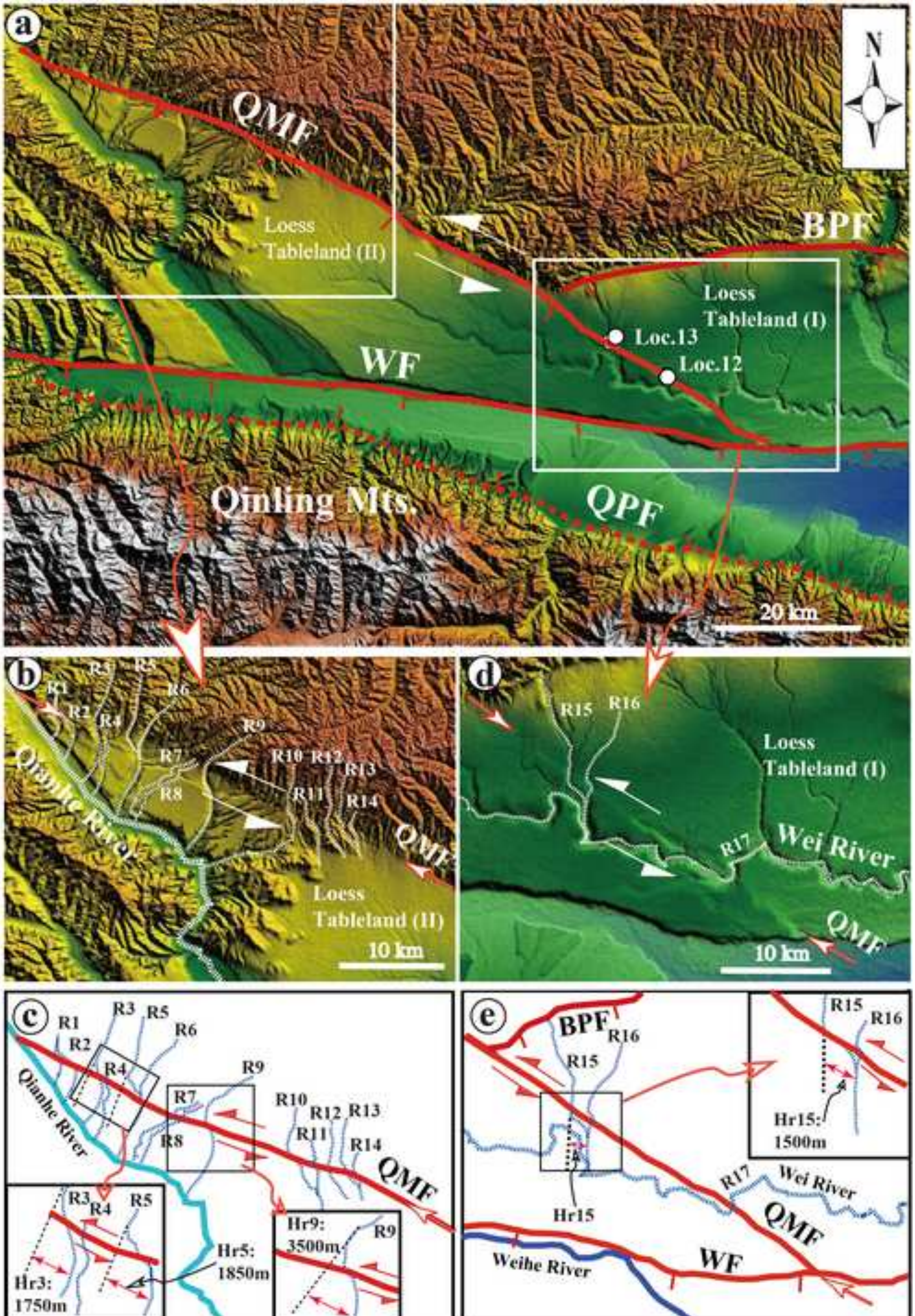

Figure13

Click here to download high resolution image

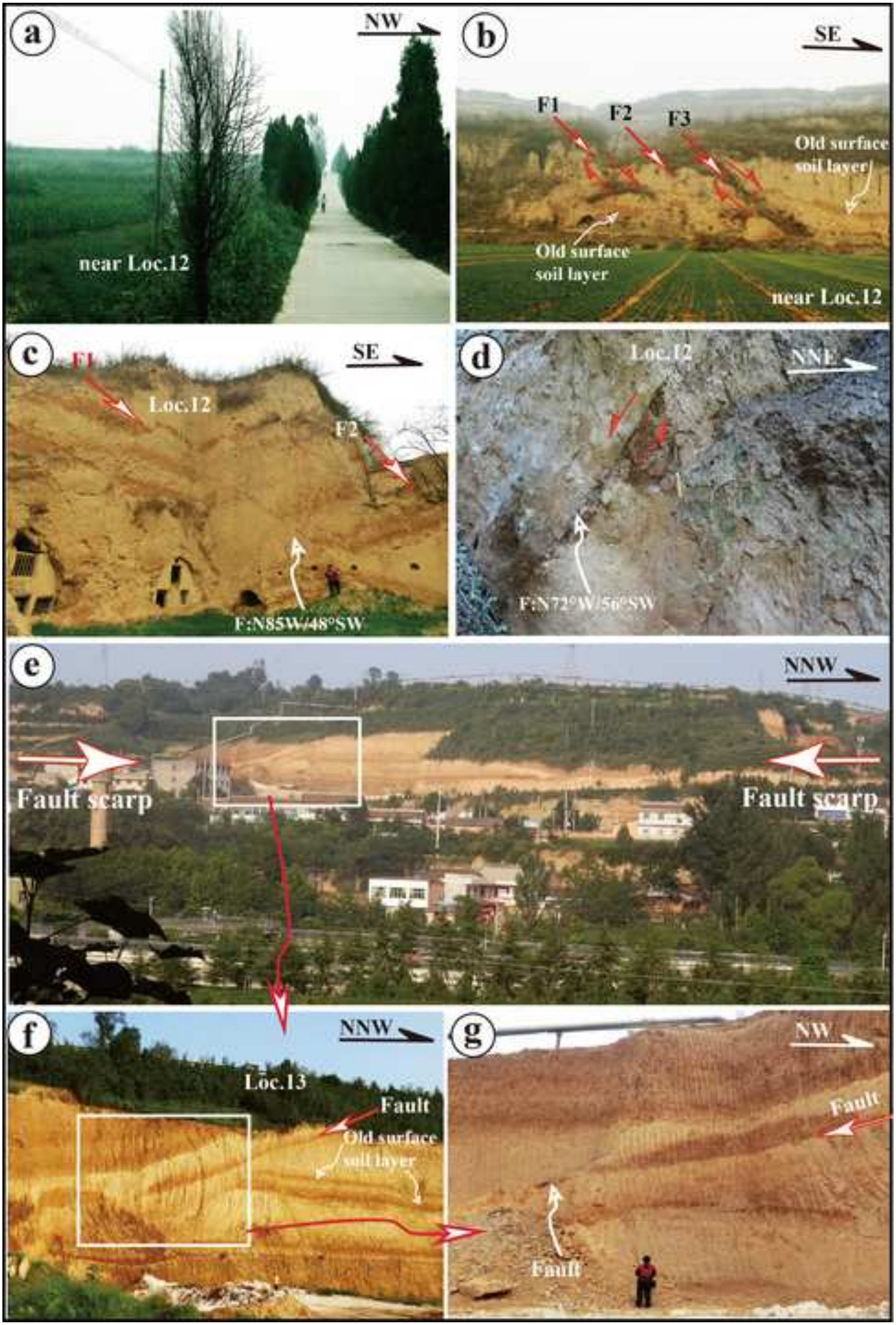

Figure14

Click here to download high resolution image

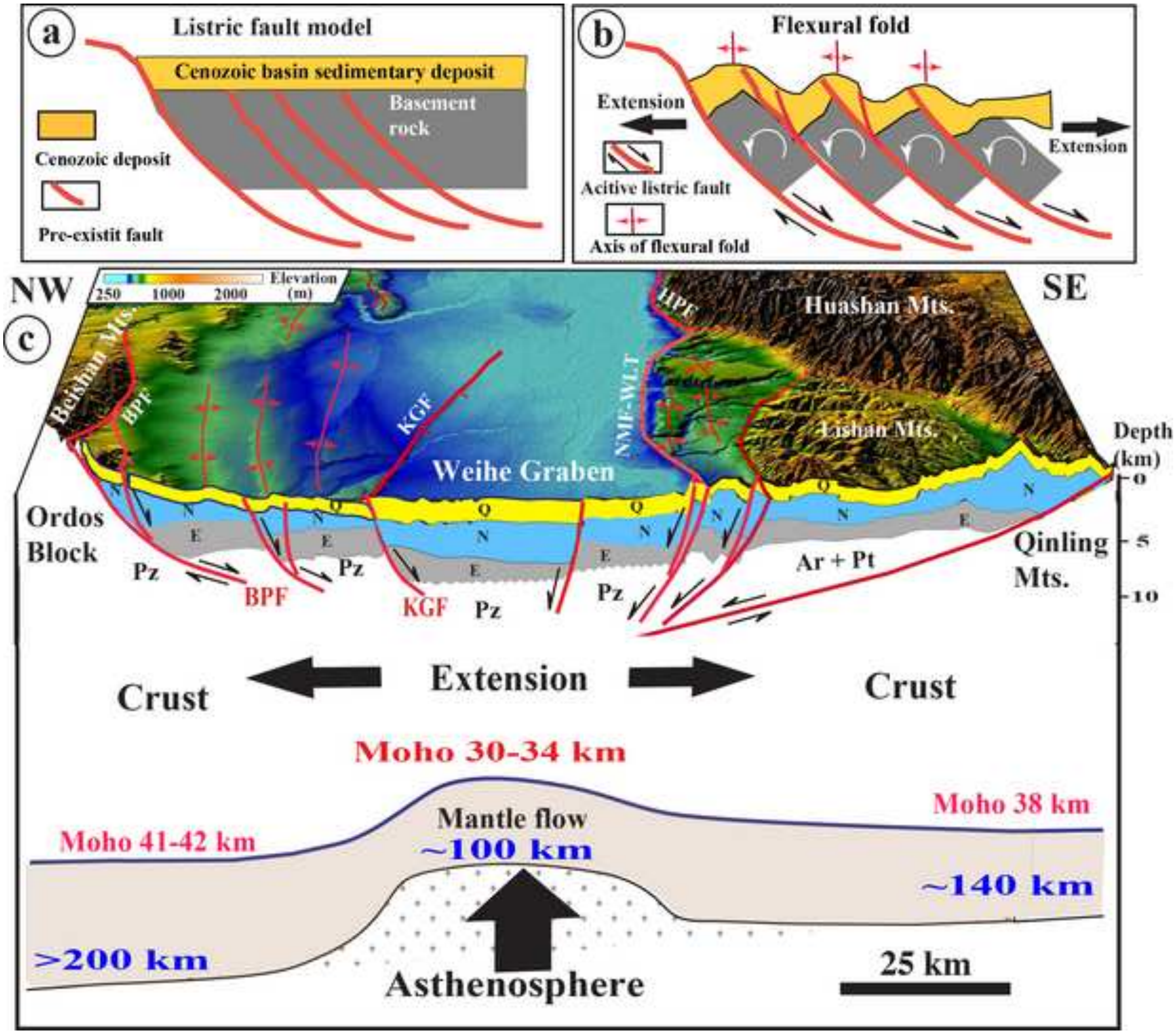

Table1

Table 1. Results of ^{14}C dating.

Sample no.	Lab no [a].	Sample material	Conventional age (yr B.P.) [c]	2σ calendar age [d]	Sampling location [e]
20120305-shell07	IAAA-120522	carbonate material	37,150± 190		Loc.6 (Fig.7d)
20120306-shell08	IAAA-120523	carbonate material	37,370 ± 20		Loc.5 (Fig.7b)
20120220-C04	Beta-335893	organic soil	3121 ± 26	BC1449-1369	Loc.7 (Fig. 9b)
20140910-C02	Beta-392138	organic soil	3520 ± 30	BC1930-1750	Loc.9 (Fig. 11b)
20140910-C01	Beta-335900	organic soil	>43,500		Loc. 8 (Fig. 5c)

[a] Samples were analyzed at Beta Analytic Inc. USA (Lab no. Beta-335893, 392138, 335900) and the Institute of Accelerator Analysis Ltd., Japan (sample nos. IAAA-120522, IAAA-120523) via accelerator mass
spectrometry (AMS).
[b] Radiocarbon ages were measured using accelerator mass spectrometry referenced to the year AD 1950. Analytical uncertainties are reported at 2σ.
[c] Conventional radiocarbon age was calculated using an assumed delta ^{13}C.
[d] Dendrochronologically calibrated calendar age using Method A from CALIB Radiocarbon Calibration Version 7.0 (Stuiver et al., 2003).
[e] Sampling location: carbonate material was taken from the alluvial sediments under the alluvial surface.

Table2

Table 2. Amounts of offset of the deflected and/or offset river channels across the QMF.

Offset River	Offset amount (m)	Offset marker
R1	1600	Loess Tablaland (I)
R2	1300	Loess Tablaland (I)
R3	1750	Loess Tablaland (I)
R4	650	Loess Tablaland (I)
R5	1850	Loess Tablaland (I)
R6	650	Loess Tablaland (I)
R7	400	Loess Tablaland (I)
R8	300	Loess Tablaland (I)
R9	3490	Boundary *
R10	1580	Mountains
R11	950	Mountains
R12	350	Mountains
R13	1200	Mountains
R14	480	Mountains
R15	1500	Loess Tablaland (I)
R16	850	Loess Tablaland (I)
R17	1000	Loess Tablaland (I)

Boundary *: Bountdary between the mountains and the Loess Tablaland (I).